



Contents lists available at ScienceDirect

Journal of Sound and Vibration

journal homepage: www.elsevier.com/locate/jsv



Research on guided wave propagation characteristics in turnout rails with variable cross-section



Rong Chen^{a,b}, Chenyang Hu^{a,b}, Jingmang Xu^{a,b,*}, Zheng Gong^{a,b}, Le Liu^{a,b}, Ping Wang^{a,b}, Xiaoping Chen^c

^a MOE Key Laboratory of High-speed Railway Engineering, Southwest Jiaotong University, Chengdu, 610031, China

^b School of Civil Engineering, Southwest Jiaotong University, Chengdu, 610031, China

^c School of Architecture and Civil Engineering, Chengdu University, Chengdu 610106, China

ARTICLE INFO

Article history:

Received 6 May 2020

Revised 12 November 2020

Accepted 16 November 2020

Available online 16 November 2020

Keywords:

Railway turnout

Variable-section waveguide

Guided wave

Propagation characteristics

ABSTRACT

Structural health monitoring based on guided waves is a promising technology that can continuously monitor and identify structural damage. Due to the variable cross-sectional characteristics of the turnout straight switch rail along the longitudinal direction of the line, it is still a challenging task to understand and clarify the guided wave propagation characteristics of the structure. In this paper, a method for analyzing the guided wave propagation characteristics of the turnout straight switch rail with variable cross-section is proposed, and the effectiveness of the method verified by finite element simulation and field experiments. The results show that the dispersion characteristics of the turnout straight switch rail change slowly along the longitudinal direction, and that at a local level the dispersion characteristics are in fact similar to rails of constant cross-section. Based on this, a three-dimensional dispersion surface with cross-sectional position information is proposed, after which the variation regularity of dispersion characteristics along the longitudinal direction is analyzed in combination with the mode shapes of the cross section at different positions. This method can provide a theoretical basis for damage detection in turnout straight switch rail, as well as for the selection of guided wave frequency and mode recognition.

© 2020 Elsevier Ltd. All rights reserved.

1. Introduction

It is of great significance to monitor the structural performance of an aging structure. In this way, damage prediction can be carried out, and the remaining service life can be predicted. Structural health monitoring (SHM) refers to the use of sensors [1,2] integrated in a structure for online, real-time acquisition of parameters that can be used to describe such health conditions as stress, strain and temperature. Then, an advanced data processing technique can be used to extract structural damage features to judge the health of the structure. The SHM technology has been widely used in recent times in the aerospace [3], machinery [4], and marine engineering [5] industry. This system is primarily composed of the following parts: a signal excitation system, a signal acquisition system, a signal analysis system, and a damage identification system. The guided wave-based SHM technology has attracted widespread attention. These waves usually have multi-mode and

* Corresponding author.

E-mail address: mang080887@163.com (J. Xu).

dispersion characteristics, making it necessary to study the theory of ultrasonic guided waves. Details on fundamentals and analysis of guided wave in different waveguides are presented in text-books on wave propagation [6–9].

For the practical application of non-destructive testing (NDT) and structural health monitoring (SHM), guided waves must be fully understood in order to achieve precise positioning of a scatterer [10–12]. Guided waves are elastic waves with multi-modes and dispersion characteristics that are formed by the existence of structural boundaries. The guided wave is, in itself, a kind of stress wave that propagates in solids. In elastic solid wave theory, a solid medium with a specific shape and boundary that can guide the propagation of stress waves is conventionally known as a waveguide. A dispersion curve can be used to describe the dispersion characteristics, mode-splitting [13,14] and speeds of guided waves at different frequencies in a medium. It can also be used to direct the NDT of guided waves, for example in terms of the selection of a guided wave mode or excitation frequency, and in the identification of modes [15]. A number of methods have been used to trace the dispersion curve, including the matrix method [16], The thin-layer method (TLM) [17–19], the finite element method (FEM) [20–22], the semi-analytical finite element (SAFE) method [23–25], the boundary FEM [26,27] and the series expansion method [28–30]. Considering the complex geometry of rail cross-sections, it is impossible to create a dispersion equation as can be done for a plate with a regular cross-section. Only a numerical method can be used to trace the dispersion curve of guided waves in rails. The most common numerical method is the finite element (FE) method. This method works by transforming the wave equation into a frequency domain equation and then introducing appropriate displacement and stress boundary conditions to solve this equation and obtain a characteristic value to trace the dispersion curve. The semi-analytical FE method can be used to develop an analytic solution in the wave propagation direction, thus greatly reducing the time required.

To develop a technology for ultrasonic guided wave-based NDT in high-speed railways, many researchers have conducted in-depth studies on the propagation characteristics of guided waves in rails with a constant cross-section. Gavric [20] traced the dispersion curve of the EU UIC861-3 rail over a range of 6 kHz using FEM, and described the characteristics of five major mode shapes. Hayashi et al. [23] studied the propagation of ultrasonic guided waves in the Japanese JIS60 rail using the SAFE method, tracing the dispersion curve of the phase velocity and group velocity of the main guided wave modes in the rail over a range of 100 kHz. After generating ultrasonic guided waves on the railhead using a contact sensor, they traced the dispersion curve of the railhead using 2-D Fourier transforms. The curve was basically the same as the dispersion curve traced by the semi-analytical method. Bartoli et al. [22] used the SAFE method to trace the dispersion curve and attenuation curve of the 115-1b AREMA rail, and also analyzed the vibration characteristics of each mode. Rose et al. [31] struck the railhead with a rail impact device in order to excite ultrasonic guided wave signals. They then collected vibration signals from the rail with an acceleration transducer testing and data analysis on the ultrasonic guided wave signals at [0–20 kHz], [20–40 kHz] and [40–60 kHz], sketching the curve of the relationship between the ultrasonic guided wave frequency and the propagation distance. Loveday [32] theoretically deduced the propagation characteristics of the guided waves in a rail with initial longitudinal stress. Duan [33] proposed a guided wave-based estimation method for the axial stress on rails.

Ultrasonic guided wave can be applied to rapid and long-distance detection of rail with the advantages of long propagation distance and large detection range [34]. Broken rails are one of the leading causes of train derailments worldwide. The relatively large number of rail breaks and resulting train derailments on South African heavy haul lines led to the development of a guided wave ultrasound (GWU) based monitoring system to detect broken rails. The system operates in pitch-catch mode with alternate transmit and receive stations permanently installed along the continuously welded rail track. A guided wave mode with energy concentrated mainly in the head of the rail allows distances of up to 2 km between the transmitter and receiver stations [35]. In order to upgrade the UBRD system to be able to detect and locate defects before the rail is completely broken, Loveday [36] installed an experimental monitoring system on the heavy haul rail track. The system consists of two transducers mounted on the rail head. By introducing artificial defects to simulate the rail head transverse defects, the system can effectively detect the rail head transverse cracks and locate at long range by a system comprising only two transducers. More recently, Ramatlo et al. [37] developed a modeling framework for ultrasonic inspection of waveguides with arbitrary discontinuities excited by piezoelectric transducers. The proposed physics-based framework can be used to efficiently perform multiple analyses considering different numbers and locations of welds, different excitation signals or to investigate the effects of changes in parameters such as transducer geometry, or material property variations caused by temperature fluctuations. The framework could therefore be used in future to set up a digital twin of a section of rail track, or in the development of a rail monitoring system by predicting reflections from defects which cannot readily be measured, but which can be simulated. Cawley [38] developed a rail defect detection technology based on guided waves, and used The Guided Ultrasonics (Rail) Ltd prototype rail testing system to effectively identify rail defects. Rose [39] proposed a technique for identifying broken rails based on elastic guided waves. Broken rail detection is possible by either utilizing an impact device or energy propagating from the train wheel in contact with the rail. Moustakidis et al. [40] proposed an automatic LRU flaw detection system based on an effective pattern recognition. By analytically investigating the influence of representative environmental conditions (temperature and humidity), a robust defect detection rate of more than 93% can be achieved. WANG et al. [41] designed an EMAT that generates 300 kHz pseudo-Rayleigh waves, and used the EMAT to detect two different types of artificial defects in a rail base specimen. Setshedi et al. [42] proposed an automatic procedure to estimate material and geometric properties of an isotropic homogeneous rail based on the Latin hypercube sampling search strategy. The procedure was developed for an elastic isotropic homogeneous rail and combined elastic moduli, density and frequency as one parameter in the eigenvalue problem. Dispersion curves were computed with different Poisson's ratio and three geometric parameters. A technique was developed to determine which semi-analytical finite element (SAFE) model

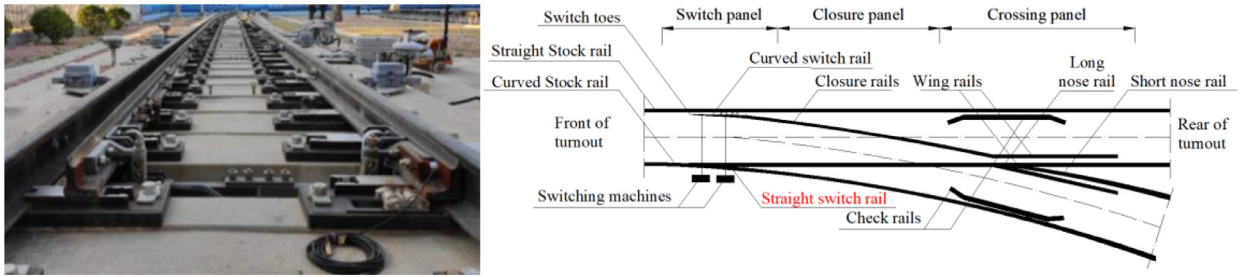


Fig. 1. CN60-1100-1:18 turnout.

best matches the experimental measurements. Sun et al. [43] Used simulated and experimental measurements, the rail defect detection was carried out. The feature parameters were extracted both from time domain and time-frequency domain. After optimizing of the feature parameter set, support vector machine method was applied to recognize and classify the rail defects. Ghabraibeh et al. [44] has identified suitable ultrasonic-guided wave modes to detect common types of defects in each part of a rail (i.e. the head, web and foot). The findings of this research demonstrated the ability to detect transverse defects as small as 2 mm and 5 mm in the head and foot, respectively. Loveday et al. [45] studied a method to estimate the modal coordinates from time domain laser vibrometer measurements using SAFE model information. The method has provided useful information for designing monitoring systems by providing estimates of the attenuation of specific modes in the field and by characterizing the performance of transducers in the lab.

Over the years, researchers have studied the propagation characteristics of guided waves in structures with a constant cross-section. However, the propagation characteristics of guided waves in structures with a variable cross-section have drawn little attention. Most studies have focused only on plate structures of varying thicknesses. Pagneux and Maurel studied the propagation of Lamb waves in an elastic waveguide with varying thickness on a theoretical basis [46]. Such work has been extended to the propagation of guided waves in a waveguide with varying curvature and variable cross-section [47]. El-Kettani et al. [48] used the FEM to study the change rule of the phase velocity and wavenumber propagating in a gradually thinned small-angle wedge-shaped elastic plate. By using the FEM, they then studied the mode conversion between the symmetric mode and the asymmetric mode in an aluminum plate whose thickness changed along the Gaussian curve [49]. In addition, they carried out theoretical research into wave propagation in an adhesively bonded composite structure with a cone-shaped adhesive layer [50]. In the existing literature [51,52] there is a technique for pulse dispersion prediction and compensation in a structure with a variable cross-section. Moreau et al. [53] estimated the wavenumber in a waveguide with linearly varying thickness. Höhne [54,55] simulated ultrasound propagation in waveguides with non-constant thickness by a multimodal approach. Krome and Gravenkamp addresses the computation of stiffness matrices for general prismatic structures with an arbitrary cross section [56]. At the same time, an approach to compute dynamic and static stiffness matrices for prismatic structures with the scaled boundary finite element method was presented. The formulation was applied to plate structures containing notches, inclined edges, delaminations or (adhesive) joints [57]. The propagation characteristics of the guided waves in a rail with a variable cross-section were primarily studied by time-domain simulation. Zhang et al. proposed an acoustic emission (AE)-based method to identify and locate new defects or extensions of existing defects on a turnout switch rail [58]. Wu et al. proposed an independent component analysis (ICA)-based ultrasonic guided wave defect detection and localization method and validated this by detecting turnout rail defects [59]. As can be seen, the research on the propagation characteristics of guided waves in turnout straight switch rail is still in the initial stage. Moreover, most studies are merely carried out from the perspective of the time domain. Although the propagation characteristics of guided waves at a particular frequency have been tested or studied through FE simulation, these fail to systematically describe the propagation characteristics of guided waves in the straight switch rail with a variable cross-section. Considering the above problem, this paper proposes a method for analyzing the propagation characteristics of guided waves in a rail with a variable cross-section. The method can be used to analyze the dispersion characteristics and mode shape of waves in the straight switch rail with a variable cross-section, the selection of a guided wave mode, the selection of an excitation frequency, and the identification of modes for NDT.

2. Methodology

2.1. The turnout switch straight rail

This paper focuses on the CN60-1100-1:18 turnout straight switch rail, which can be seen in Fig. 1. Turnouts (switches and crossings) are essential components of railway infrastructure, providing flexibility to traffic operation. They consist of a switch panel, a crossing panel and a closure panel. To enable the vehicle to change between tracks, the profiles of switch rails and crossing rails are designed to vary along the switch and crossing panels. The straight switch rail head needs to be cut horizontally and vertically [60], as shown in Fig. 2. The straight switch rail bottom needs to be cut horizontally. The turnout is a vulnerable spot in a railway and an important yet difficult point of maintenance. There is currently a lack of

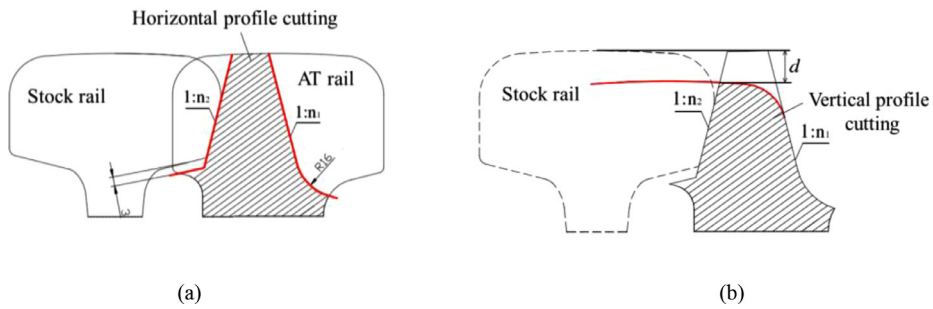


Fig. 2. Schematic diagram of straight switch rail cutting: (a) Horizontal profile cutting; (b) Vertical profile cutting.

effective methods for straight switch rail monitoring, so it is necessary to study the propagation characteristics of its guided waves.

2.2. Proposed method

The propagation of guided waves in a waveguide with a slowly-varying cross-section is a challenging problem, since the dispersion characteristics of the guided wave modes are not only frequency-dependent, but also cross section-dependent. This means that the wave number, phase velocity and group velocity are variable in each wave mode. At present, there is no effective numerical method that can be used to reveal the dispersion characteristics of the straight switch rail with a variable cross-section, so switch rail damage cannot be tested effectively. To study the dispersion characteristics of guided waves in the straight switch rail with a variable cross-section, we should first create a reasonable numerical method that can be used to analyze the dispersion characteristics of elastic waves in the straight switch rail with a variable cross-section. The dispersion characteristics of the waveguide are directly related to the cross-sectional shape. Considering that the actual cross-section of the straight switch rail with variable cross-section changes in a slow yet continuous manner, and that the propagation characteristics of guided waves become locally equivalent to that of a rail with a constant cross-section. By comparing the dispersion curves of each cross section, **it is found that the dispersion curve between two similar cross sections was basically the same**. Simulation results showed that the modes that were studied were found to change smoothly and continuously in the straight switch rail with variable cross-section.

First of all, the straight switch rail with variable cross-section was divided into $n-1$ ($n \geq 1$) segments longitudinally, with the inter-sectional spacing able to reveal the continuous longitudinal change of the rail section. The dispersion curves of the n cross-sections of the rail were also sketched. The dispersion curves of guided waves that were similar in mode on different sections were then fitted into a three-dimensional (“wavenumber-frequency-position”) dispersion surface based on longitudinal position, as shown in Fig. 3. The dispersion surface presents the dispersion curves of cross-sections in different positions and the longitudinal change rule of the frequency dispersion characteristics of waves similar in mode. After this, the propagation regularity of guided waves in the straight switch rail with variable cross-section was further studied based on the mode shape corresponding to the “wavenumber-frequency-position” points on the dispersion surface. The dispersion characteristics of the cross-sections were calculated using the SAFE method.

3. Numerical study

3.1. Mode shape tracking

This paper analyses the straight switch rail on a CN60-1100-1:18 turnout. The variable cross-section rail segment was 10,962 mm long and the head width changed from 0 mm to 72.2 mm. Typical sections were selected by taking a head width of 5 mm as a step distance, before using the SAFE method to trace the dispersion curve of each cross-section. The material density was 7850 kg/m, the elasticity modulus was 210 GPa and Poisson's ratio was 0.3. The dispersion curves of three typical cross-sections of the straight switch rail were selected for comparative analysis. The rail head widths of three typical cross-sections were 30 mm, 35 mm and 40 mm, respectively. The cross-section shape and dispersion curves are shown in Fig. 4. As can be seen in this figure, similar cross-sections correspond to similar dispersion curves. As can be seen in Fig. 4(d), there exist mode repulsion, and when dispersion curves pass through the 31 kHz zone, the mode shapes are effectively swapped around. In this zone, various mode shapes form an approximate linear combination of the mode shapes outside the zone.

Fig. 5 shows the change rule for dispersion curves corresponding to Mode 1, Mode 2 and Mode 6 along the longitudinal direction of the straight switch rail. To describe this change intuitively, the wave mode conversion on the dispersion curves is not considered here, while waves of similar mode shape are considered to be of the same mode. The guided wave modes corresponding to different straight switch rail cross-sections and their mode shapes at 30 kHz are shown in Figs. 6–8. The in-plane mode shape is expressed in deformation while the out-plane mode shape is expressed in color. Mode 1, Mode 2 and

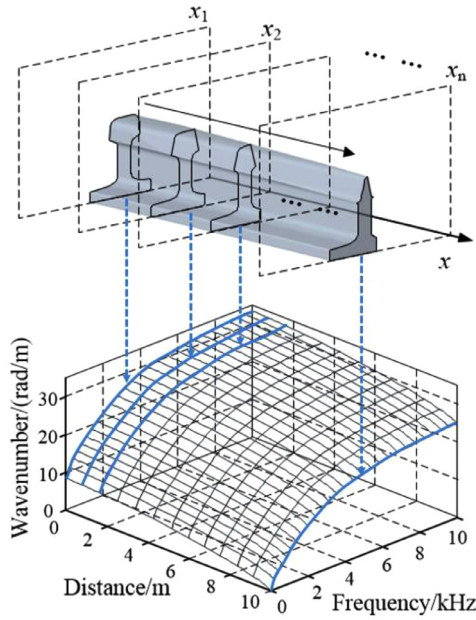


Fig. 3. Creation of the dispersion surface.

Mode 6 are used to explain the dispersion characteristics of the straight switch rail with a variable cross-section. As can be seen in Figs. 5(a) and 6, the guided waves at the rail bottom corresponding to Mode 1 are similar in mode shape. Moreover, there is no difference in shape or material parameters among the deformation position on different straight switch rail sections. As a result, there is no change in the dispersion curve corresponding to Mode 1. As can be seen in Figs. 5(b) and 7, the dispersion curve corresponding to Mode 2 changes slowly with straight switch rail cross-sections, as does the guided wave mode shapes. As can be seen in Figs. 5(c) and 8, the dispersion curve corresponding to Mode 6 changes slowly with straight switch rail cross-sections, as does the guided wave mode shapes. When the mode shape is located on a variable cross-section area, the dispersion curve and mode shape corresponding to the wave mode will change slowly with position; when the mode shape is located on a non-variable cross-section area, the dispersion curve and mode shape corresponding to the wave mode will not change with position.

3.2. Simulation of the generation of mode 1 and mode 2

To verify the validity of the analytical method, we designed two guided wave verification simulations for the straight switch rail. An FE model of the straight switch rail was built to excite guided wave modes. Guided wave excitation was performed on the cross section of the straight switch rail with a rail head width of 35 mm. The excitation positions of the expected wave modes (Mode1 and Mode 2) were then determined according to the analysis of mode shape on the cross section with a head width of 35 mm. The 2D Fourier Transform (2D-FFT) was used to trace the dispersion curve on the typical cross-section of the straight switch rail. Then, the above dispersion curve was compared with the wave number-frequency dispersion curve sketched by analyzing the characteristics of guided waves in the straight switch rail with a variable cross-section, validating the method's effectiveness.

3.2.1. Analysis of dispersion characteristics

The dispersion curves and mode shapes on the cross-section with a rail head width of 35 mm were calculated using the SAFE method. Fig. 9 shows the mode shape at 30 kHz. The out-plane mode shape is expressed in color and represented by the RAINBOW legend. Different guided wave modes correspond to the same color scale. The colors of Mode 1 to Mode 9 (the naming method is sorted by wave number from largest to smallest) are relatively consistent, and those wave modes show in-plane deformations. Mode 10 to Mode 15 is mainly out-of-plane deformation.

3.2.2. Simulation description

In this study, ANSYS/LS-DYNA was used to simulate the propagation of guided waves in the straight switch rail. The stability of numerical solutions was determined by both time and spatial resolution. The time marching step was obtained from the Courant–Friedrichs–Lowy (CFL) number requirement. To avoid numerical instability, the stability limit of the integration time step was made equal to

$$\Delta t = \frac{L_{\min}}{C_L} \quad (1)$$

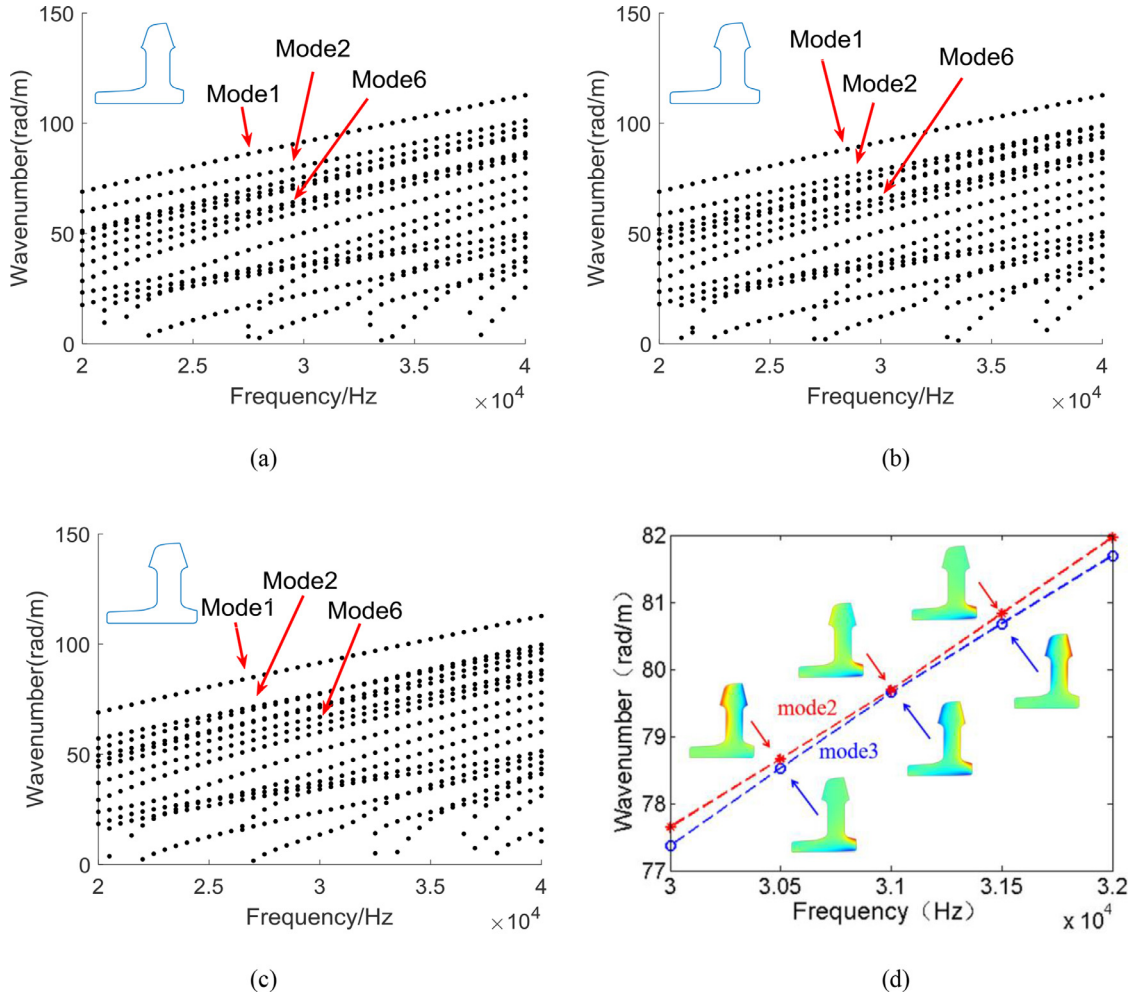


Fig. 4. Wave number-frequency curves: Cross-sections with (a) 30 mm rail head width; (b) 35 mm rail head width; (c) 40 mm rail head width; (d) 40 mm rail head width (detailed view).

Table 1
Position of key cross-sections in the model.

Rail head width (mm)	0	5	10	15	20	25	30
Distance from the tip of the turnout switch rail (m)	0	0.961	1.925	2.889	3.852	4.814	5.764
Rail head width (mm)	35	40	45	50	60	65	72.2
Distance from the tip of the turnout switch rail (m)	6.584	7.319	7.984	8.614	9.753	10.269	10.962

where L_{\min} represents the minimum size of the minimum model element and C_L represents the velocity of the longitudinal waves passing through the material. This limit represents the time that the longitudinal waves take to pass through the element.

The maximum frequency f_{\max} of the dynamic problem limits the integration time step and element size. At least 20 points [61] are used in every cycle at the maximum frequency, i.e.,

$$\Delta t = \frac{1}{20f_{\max}} \quad (2)$$

The size L_e of the FE meshes is usually calculated according to the minimum wavelength L_{\min} of the object being analyzed. The spatial resolution usually requires 10 nodes [62] for each wavelength, i.e.,

$$L_e = \frac{\lambda_{\min}}{10} \quad (3)$$

Fig. 10 shows a solid 3-D element model of the straight switch rail. Typical cross-sectional positions are shown in Table 1. In the simulation, the density of the straight switch rail material was set to 7850 kg/m^3 , the Young's modulus was set to

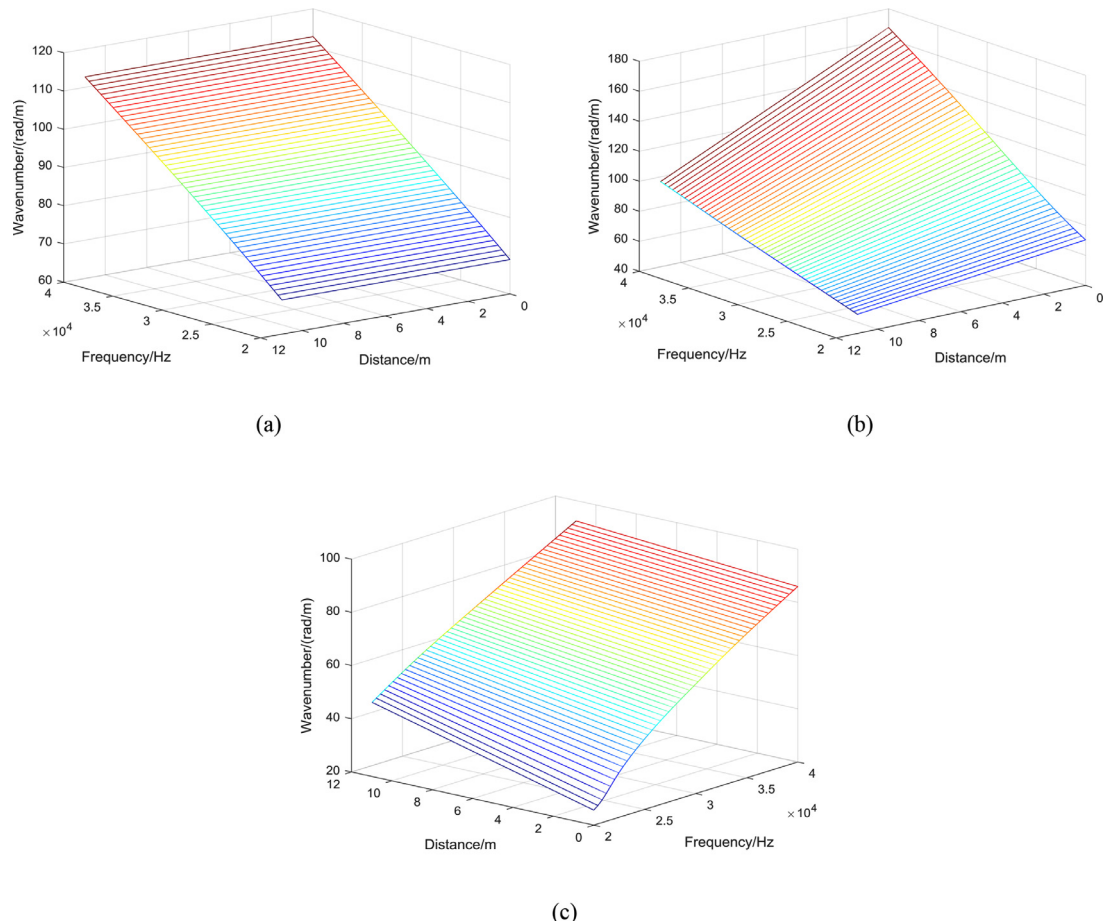


Fig. 5. Wave number-frequency surface: (a) Mode 1; (b) Mode 2; (c) Mode 6.

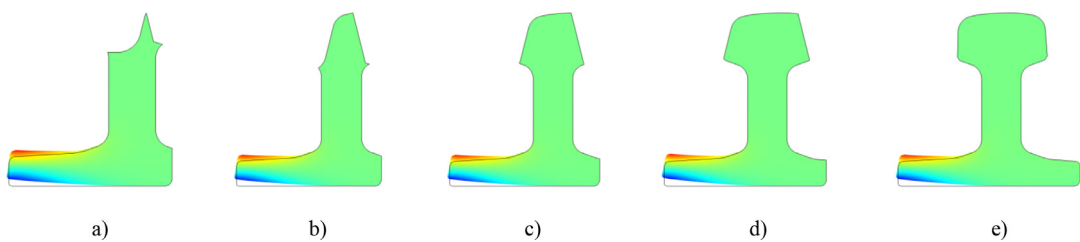


Fig. 6. Mode shape of Mode 1 at 30 kHz: (a) Cross-section with 0 mm rail head width; (b) Cross-section with 20 mm rail head width; (c) Cross-section with 40 mm rail head width; (d) Cross-section with 60 mm rail head width; (e) Cross-section with 72.2 mm rail head width.

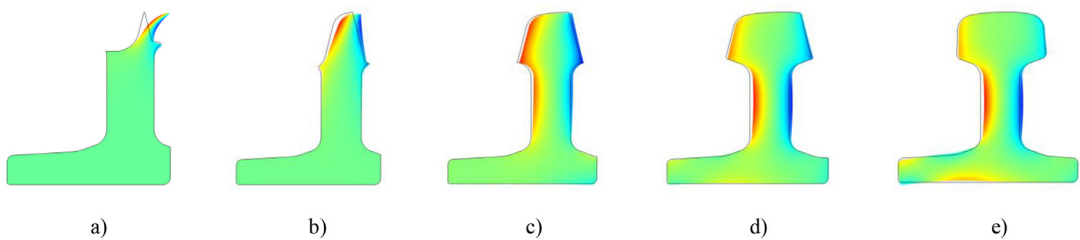


Fig. 7. Mode shape of Mode 2 at 30 kHz: (a) Cross-section with 0 mm rail head width; (b) Cross-section with 20 mm rail head width; (c) Cross-section with 40 mm rail head width; (d) Cross-section with 60 mm rail head width; (e) Cross-section with 72.2 mm rail head width.

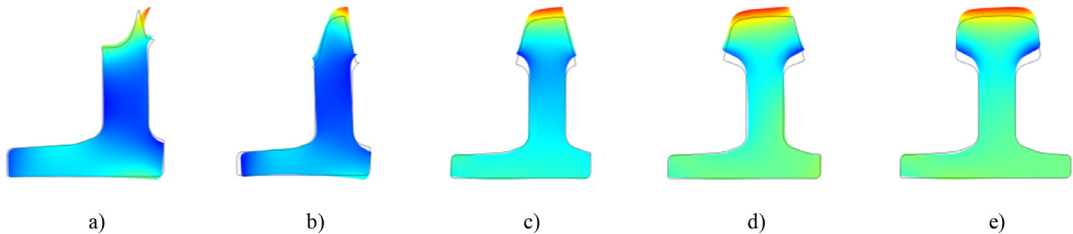


Fig. 8. Mode shape of Mode 6 at 30 kHz: (a) Cross-section with 0 mm rail head width; (b) Cross-section with 20 mm rail head width; (c) Cross-section with 40 mm rail head width; (d) Cross-section with 60 mm rail head width; (e) Cross-section with 72.2 mm rail head width.

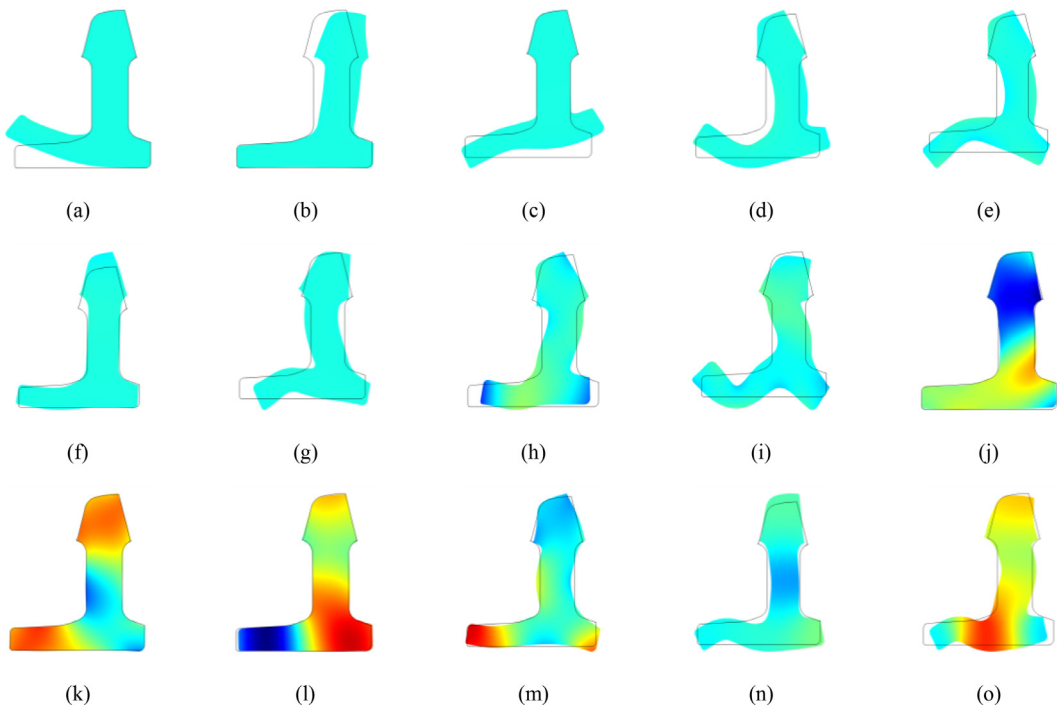


Fig. 9. Mode shapes corresponding to different wave modes at 30 kHz: (a) Mode 1; (b) Mode 2; (c) Mode 3; (d) Mode 4; (e) Mode 5; (f) Mode 6; (g) Mode 7; (h) Mode 8; (i) Mode 9; (j) Mode 10; (k) Mode 11; (l) Mode 12; (m) Mode 13; (n) Mode 14; (o) Mode 15.

210 GPa and the Poisson's ratio was set to 0.3. In this paper, an 8-node hexahedral element is used to mesh the 3D solid element model of the straight switch rail. The grid size is 3 mm, and the integration time step is 6×10^{-7} s.

The excitation signal is a 10-period sine wave signal with a center frequency of 30 kHz modulated by the Hanning window, as shown in Fig. 11. Fig. 12 shows the vertical and lateral excitation positions of the cross section of the straight switch rail with a head width of 35 mm. Fig. 12(a) shows the mode shape (vertical displacement amplitude) of the outer outline at a frequency of 30 kHz. The abscissa represents the node number. The nodes are the discrete points on the rail outline. With the head position as the initial node, the discrete points are sorted anticlockwise along the profile. Fig. 12(b) shows the position of the excitation nodes selected in Fig. 12(a) on the profile. Based on the literature [63] Mode 1 has the largest amplitude at Node 54 shown in Fig. 12, while the amplitude of the other wave modes approaches 0. So, Mode 1 can be effectively excited at this node owing to its large amplitude, while there are only a very small number of other wave modes that can be excited due to their relatively low amplitude. Fig. 12(c) shows the mode shape (lateral displacement amplitude) of the outline at a frequency of 30 kHz. Fig. 12(d) shows the position of the excitation nodes selected in Fig. 12(c). Mode 2 has the largest amplitude at Node 15, as shown in Fig. 12(c), while the amplitude of the other wave modes approaches 0. Therefore, Mode 2 can be effectively excited at this node owing to its large amplitude. A group of displacement data acquisition arrays are set ± 1 m away from the nodes on the cross sections of the straight switch rail with a head width of 10, 15, 20, 25 and 30 mm. The data acquisition nodes are 3 mm away from each other, as shown in Fig. 13(c). The pickup signal node position is shown in Fig. 13. The cross section with a head width of 30 mm is taken as an example for a description: The Mode 1 and Mode 2 signals can be picked up effectively at those positions, while the amplitude of the other wave modes remains low.

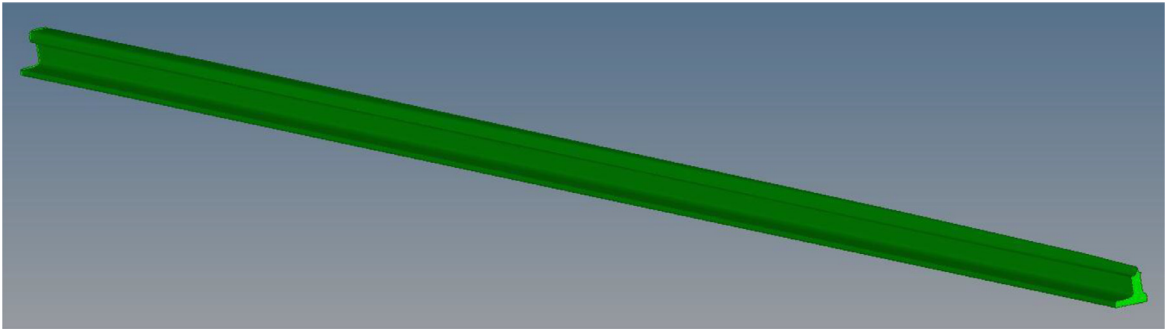


Fig. 10. FE model of the straight switch rail.

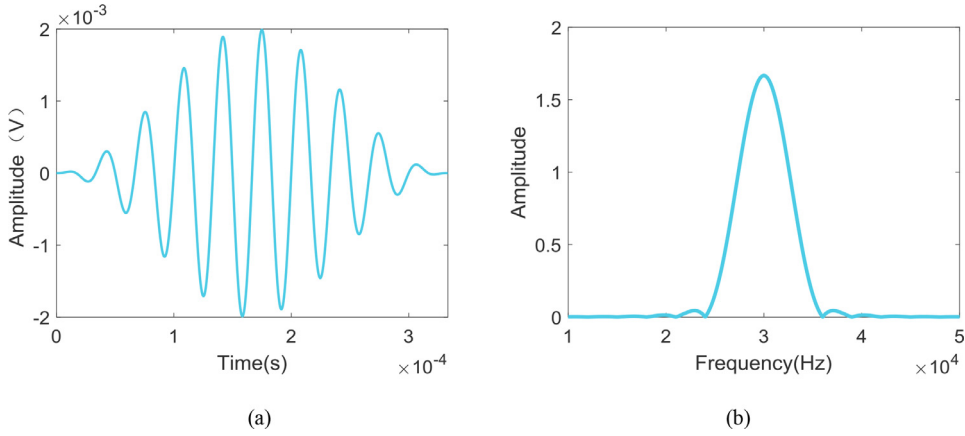


Fig. 11. Excitation signal: (a) Time domain; (b) Frequency domain.

3.2.3. Numerical results

Figs. 14 and 15 show the vertical and lateral displacements nephograms extracted from the simulation calculation results. As shown in Fig. 14, the guided waves propagate at the bottom of the rail. As shown in Fig. 15, the guided waves mainly propagate at the head of the rail.

Taking the cross section with a head width of 20 mm as an example, the vertical and lateral displacements signals of the nodes located within ± 1 m on this cross section were combined in the order of spatial position scanning to reveal time-space wave-field signals. The results are shown in Figs. 16 and 17. As can be seen in Figs. 16 and 17, the guided wave signals received during scanning are primarily composed of a principal wave packet.

The wave modes were named according to wavenumber, from high to low, i.e., Mode 1, Mode 2 etc. The results extracted were processed by 2D-FFT and transformed into a frequency-wavenumber-amplitude domain. After this, the dispersion curve could be traced by the SAFE method and compared with the results of 2D-FFT. The simulation results of the generation of Mode 1 and Mode 2 are shown in Figs. 18 and 19. As can be seen, the results are very consistent with the dispersion curve of Mode 1 in Fig. 18(a), (b) and (c) and Mode 2 in Fig. 18(d) and (e). The results are very consistent with the dispersion curve of Mode 2 in Fig. 19(a), (b) and (c) and Mode 1 in Fig. 19(d) and (e).

The time-domain waveforms of the vertical and lateral displacements of the nodes on the cross sections of the straight switch rail with a head width of 30, 25, 20, 15 and 10 mm were wavelet-transformed and compared with the theoretical time-frequency curve. The theoretical time-frequency curves corresponding to the first 2 wave modes were selected only by reference to the comparison results in Figs. 20 and 21. The theoretical time-frequency curve at the maximum energy level is shown as a bold line in Figs. 20 and 21. Fig. 20(a), (b) and (c) correspond to Mode 1; Fig. 20(d) and (e) correspond to Mode 2. This is the same as the results shown in Fig. 18. Fig. 21(a), (b) and (c) correspond to Mode 2; Figs. 21(d) and (e) correspond to Mode 1. This is the same as the results in Fig. 19. The group velocity changed with the gradual change in cross section. The variation of group velocity is considered in the calculation of the theoretical time-frequency curve. For example, for the rail section corresponding to cross-sections with a rail head width of between 35 and 30 mm, a cross-section of 35 mm has been used for the theoretical calculations and therefore their group velocity has been used as input. Other rail sections are treated the same as above.

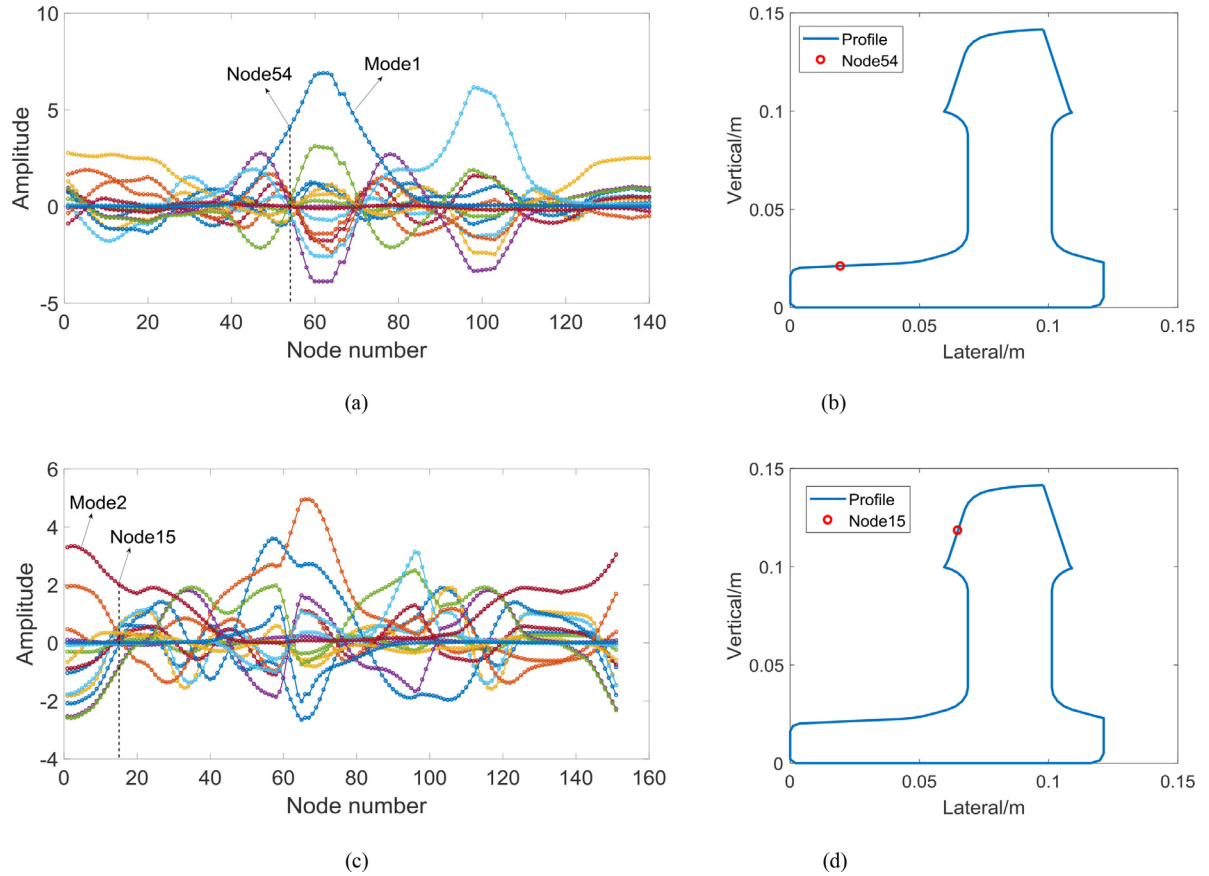


Fig. 12. Excitation position on the cross section with a head width of 35 mm: (a) Mode shape-vertical displacement; (b) Excitation position of mode 1; (c) Mode shape-lateral displacement; (d) Excitation position of mode 2.

4. Experimental results and comparison

4.1. Experimental set-up

To verify the validity of the analytical method, we designed a guided wave verification experiment for the straight switch rail. Fig. 22 shows the schematic diagram of the experimental system. The power amplifier amplifies a low-voltage signal from the function generator to a high-voltage signal and causes the transmitting sensor to excite elastic waves. The receiving sensor then converts the mechanical waves transmitted through the rail into a low-voltage signal. Finally, the acquisition system collects and stores the electrical signals processed by the filtering and amplification system.

The system consists of a signal generator, and a signal reception and display unit. The signal generator is used to generate and amplify excitation signals, thus exciting the structure. The signal reception and display unit receives and processes preliminary response signals from the structure. The unit components and key equipment are shown in Fig. 23. The test equipment includes the HP33120A function generator, the Soundwel NI Pxle-1071 data acquisition system, Soundwel ATA-2022H high voltage amplifier, and Soundwel SR150N ultrasonic sensor.

Measured points were arranged 8344mm-9344mm away from the straight switch rail. Guided wave excitation and signal pickup were performed at the bottom of the rail, and the excitation position is shown in Fig. 25. There were 5 signal pickup positions altogether, spaced at an interval of 0.2 m. The measured points and sensor arrangement are shown in Fig. 24. A vertical excitation signal was applied at the excitation location. The excitation signal was a 10-cycle sine wave with a center frequency of 30 kHz modulated by the Hanning window, and the peak value is 300 mV. The amplification power of the power amplifier is 30 W.

In order to clarify the wave mode excited in the experiment, a simulation is performed here. An FE model of the straight switch rail was created. The same measured points as those selected in the experiment were adopted for excitation and reception, and the calculated results compared with the experimental results. During the simulation, the density of the turnout rail material was set to 7850 kg/m^3 , the Young's modulus was set to 210 GPa and the Poisson's ratio was set to 0.3.

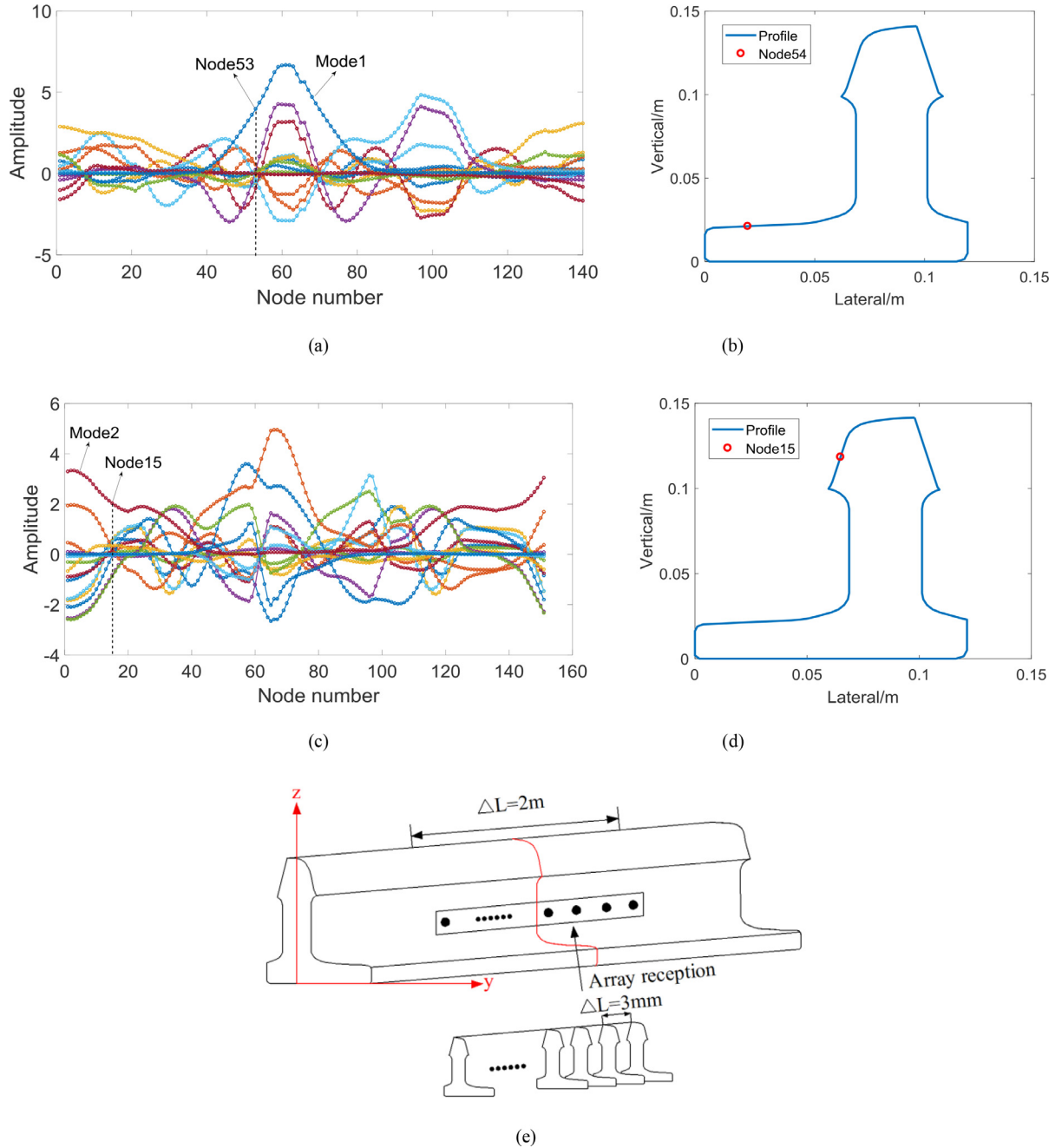


Fig. 13. Signal pickup position on the cross section with a head width of 30mm: (a) Mode shape-vertical displacement; (b) Signal pickup position of mode 1; (c) Mode shape-lateral displacement; (d) Signal pickup position of mode 2; (e) Schematic diagram of data acquisition arrays.

In this paper, an 8-node hexahedral element was used to mesh the 3D solid element model of the turnout. The mesh size is 2 mm.

4.2. Experimental results

As shown in Fig. 26, guided wave energy is concentrated at the bottom of the rail. The vertical displacement signals are located within ± 0.6 m of the signal pickup position at the rail bottom, 1 m away from the excitation point. They were combined in the order of their spatial position scanning to reveal time-space wave Field signals. The results are shown in Fig. 27. As can be seen, the guided wave signal received during scanning consists of a principal wave packet. The results

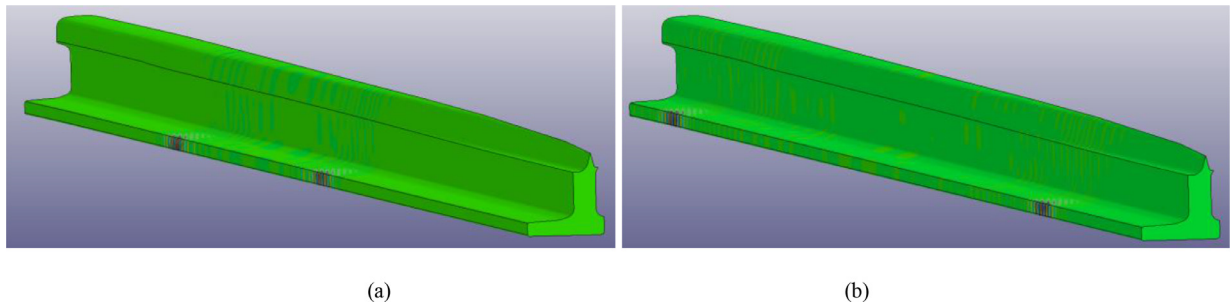


Fig. 14. Vertical displacement nephogram of mode 1: (a) 0.00075 s; (b) 0.00166 s.

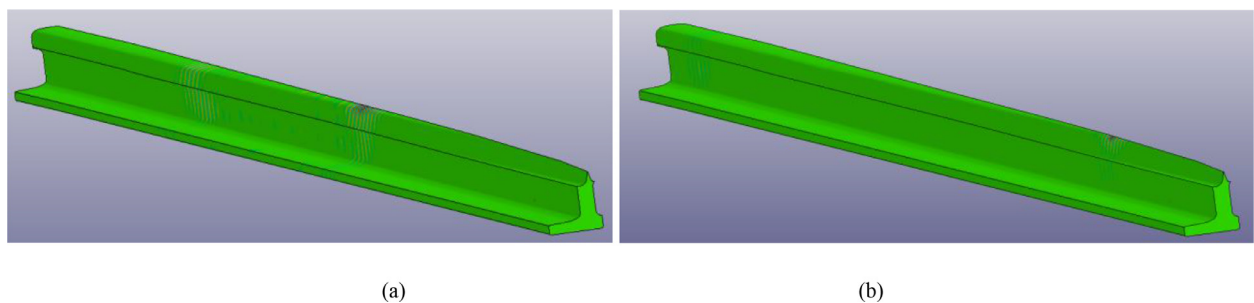


Fig. 15. Lateral displacement nephogram of mode 2: (a) 0.00075 s; (b) 0.00166 s.

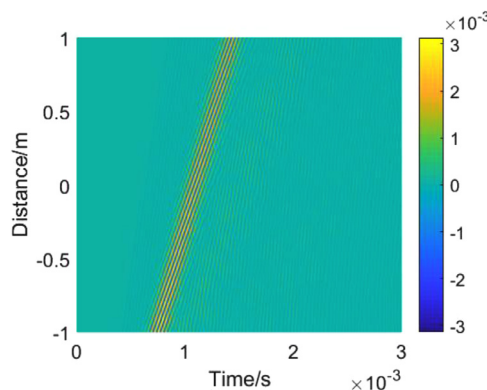


Fig. 16. Time-space wave-field signal of mode 1.

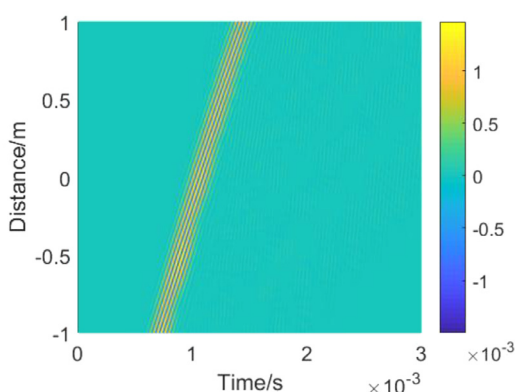


Fig. 17. Time-space wave-field signal of mode 2.

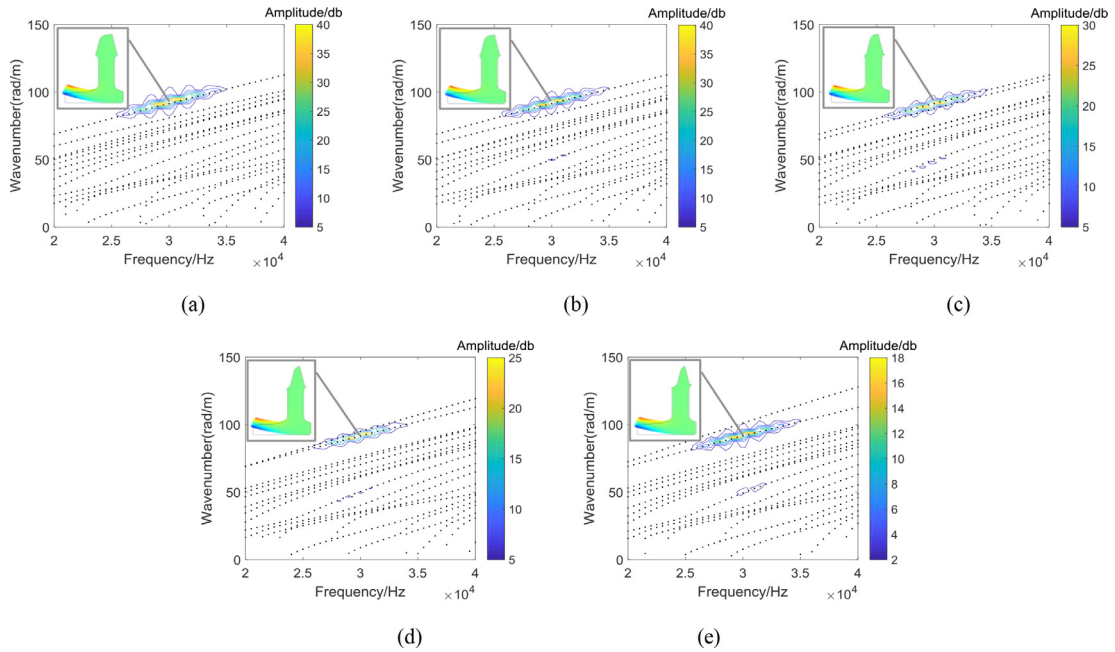


Fig. 18. Dispersion curve (simulation of the generation of mode 1): (a) Cross-section with 30 mm rail head width; (b) Cross-section with 25 mm rail head width; (c) Cross-section with 20 mm rail head width; (d) Cross-section with 15 mm rail head width; (e) Cross-section with 10 mm rail head width.

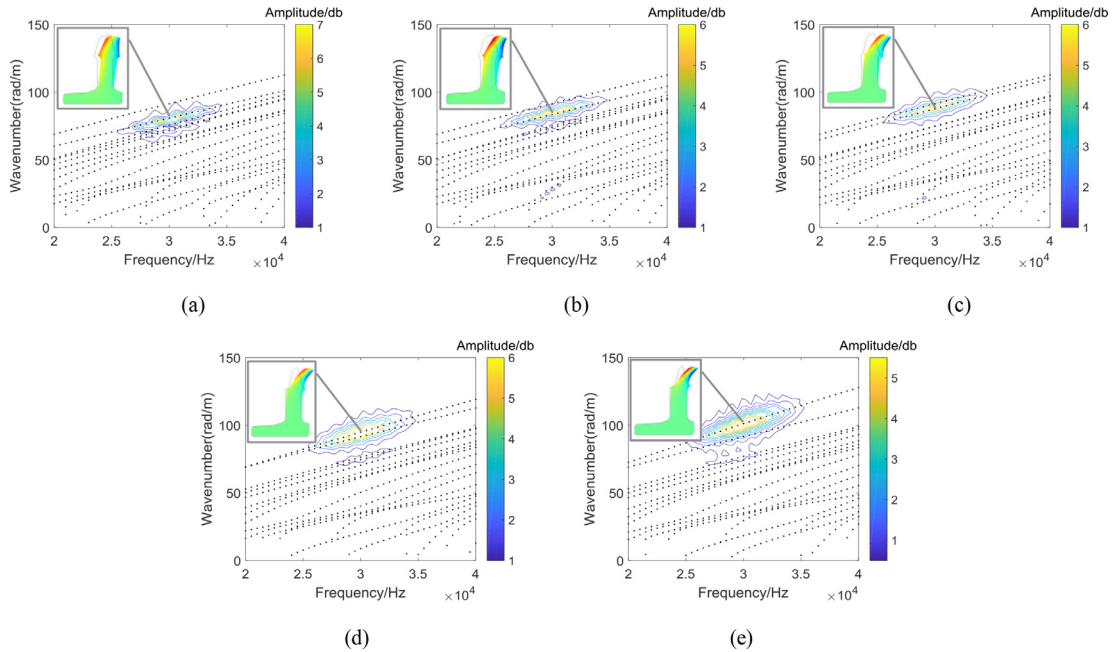


Fig. 19. Dispersion curve (simulation of the generation of mode 2): (a) Cross-section with 30 mm rail head width; (b) Cross-section with 25 mm rail head width; (c) Cross-section with 20 mm rail head width; (d) Cross-section with 15 mm rail head width; (e) Cross-section with 10 mm rail head width.

extracted were processed by 2D-FFT and transformed into a frequency-wavenumber-amplitude domain. After this, the dispersion curve traced by the semi-analytical FE method was compared with the results of the 2D-FFT. The results are shown in Fig. 28. As shown by these results, it is fully in agreement with the dispersion curve of Mode 1 in Fig. 28, while its group velocity at 30 kHz is equal to 2893 m/s.

Fig. 29 shows the test data generated by 20–40 kHz band-pass FFT filtering and normalization processing. The guided wave signal is predominantly a principal wave packet. The group velocity of the guided waves was calculated by the maximum amplitude method, equal to about 2938 m/s, basically the same as that of Mode 1. Fig. 30 shows the data of the

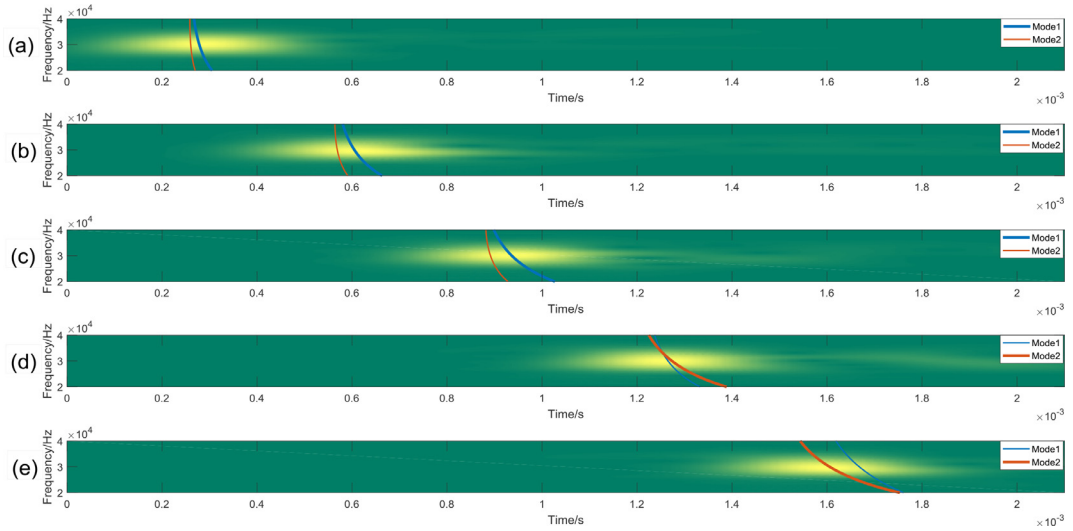


Fig. 20. Time-frequency curve for group velocity (simulation of the generation of mode 1): (a) Cross-section with 30 mm rail head width; (b) Cross-section with 25 mm rail head width; (c) Cross-section with 20 mm rail head width; (d) Cross-section with 15 mm rail head width; (e) Cross-section with 10 mm rail head width.

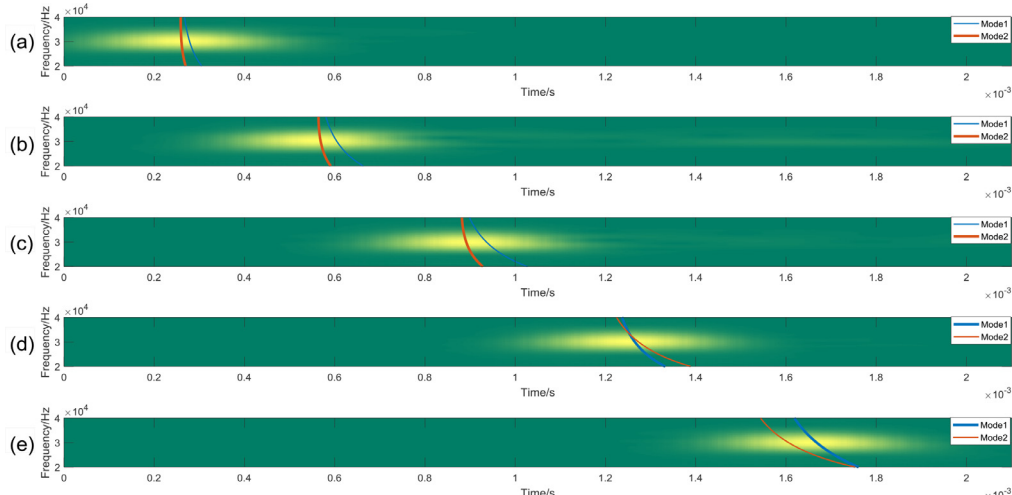


Fig. 21. Time-frequency curve of phase velocity (simulation of the generation of mode 2): (a) Cross-section with 30 mm rail head width; (b) Cross-section with 25 mm rail head width; (c) Cross-section with 20 mm rail head width; (d) Cross-section with 15 mm rail head width; (e) Cross-section with 10 mm rail head width.

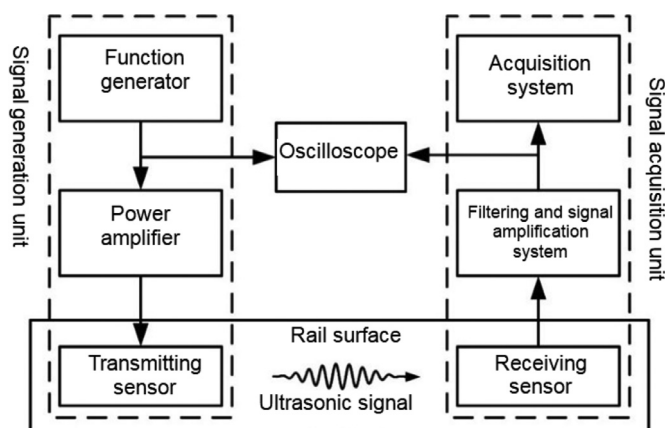


Fig. 22. Schematic diagram of the experimental system.



Fig. 23. Key experimental equipment: (a) Signal generator/acquisition unit; (b) Sensor.

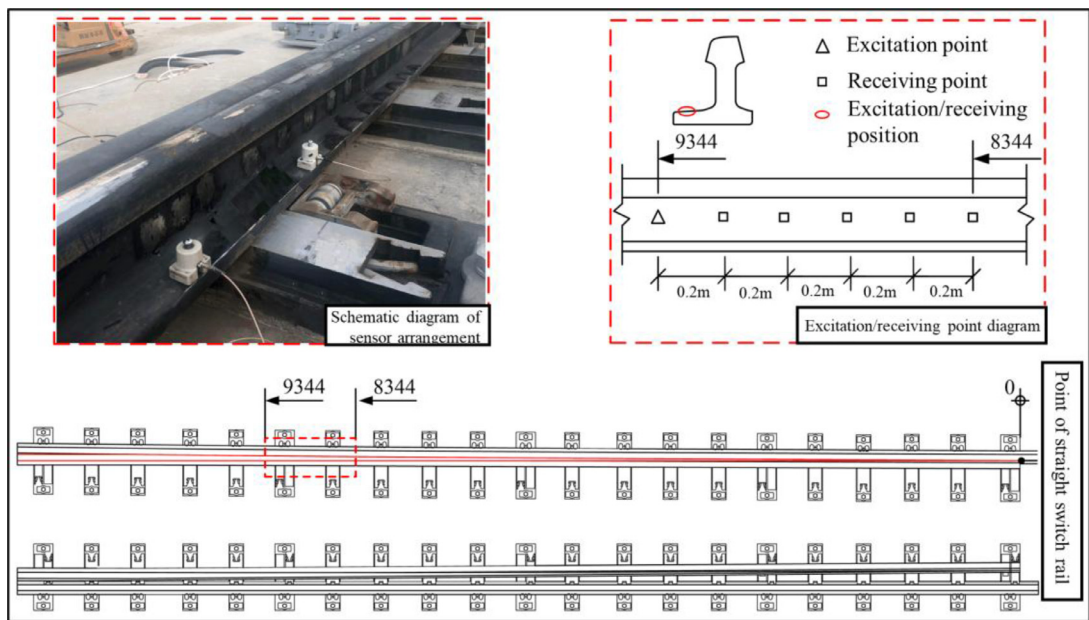


Fig. 24. Arrangement of measured points on the rail with variable cross-section and sensors.

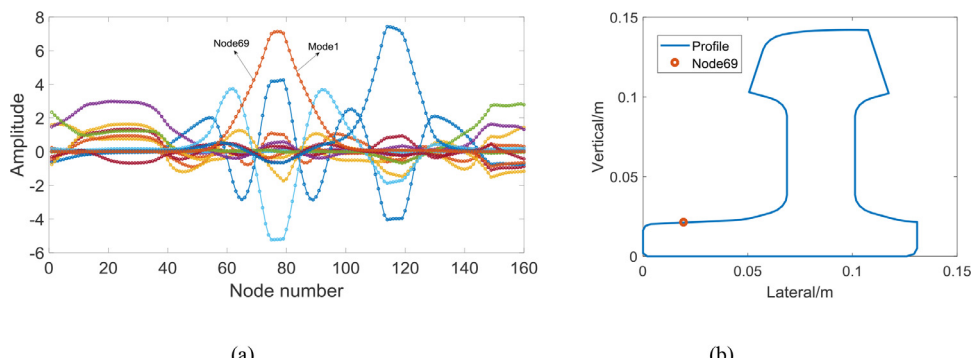


Fig. 25. Excitation position: (a) Mode shape-lateral displacement; (b) Excitation position.

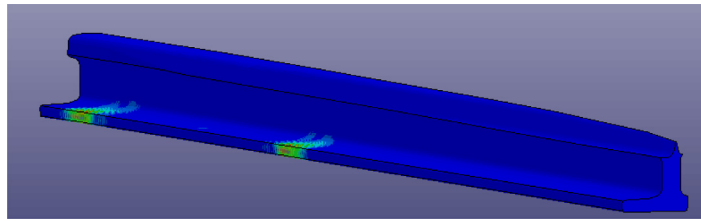


Fig. 26. Stress nephogram of guided waves.

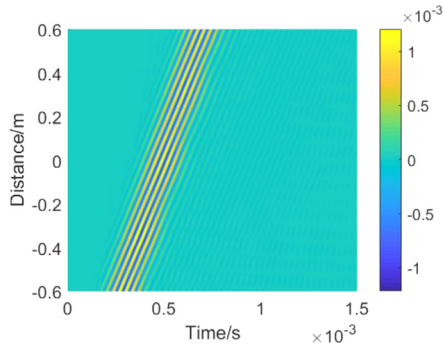


Fig. 27. Time-space wave-field signals of mode 1.

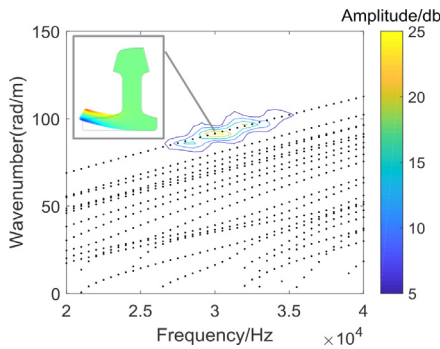


Fig. 28. Dispersion curve.

testing and simulation normalization processing conducted 1 m away from the excitation point. The results show that the two are in good agreement with each other. The time-domain waveform of the test was wavelet-transformed and compared with the theoretical time-frequency curve of Mode 1. As shown by the results in Fig. 31, the two are in good agreement with each other.

5. Conclusion and future work

This paper proposes a method for analyzing the propagation characteristics of guided waves in the turnout switch rail. The method considers the influence of variable cross-section characteristics on the propagation characteristics of guided waves. The following conclusions can be drawn:

- (1) The dispersion characteristics and mode shape of guided waves changed slowly along the longitudinal direction of the straight switch rail. The article shows the change characteristics of the dispersion curve and mode shape in the straight switch rail. To be specific, Mode 1 mainly manifested itself as a vertical deformation of the rail bottom, Mode 6 mainly manifested itself as a vertical deformation of the rail head, while Mode 2 manifested itself as a lateral deformation of the rail web and railhead. Since the cross section of the rail bottom on the working side did not change, the dispersion curve and mode shape corresponding to Mode 1 also did not change with position. Because the railhead was cut, the dispersion curve and mode shape of Mode 2 and Mode 6 changed with position.
- (2) ANSYS/LS-DYNA was used to simulate the propagation of guided waves in the straight switch rail. After an analysis of the mode shape, an appropriate excitation position was selected for excitation of the desired wave modes (Mode 1 and Mode 2). Guided wave signals were extracted from different positions to trace the dispersion curve of the typical

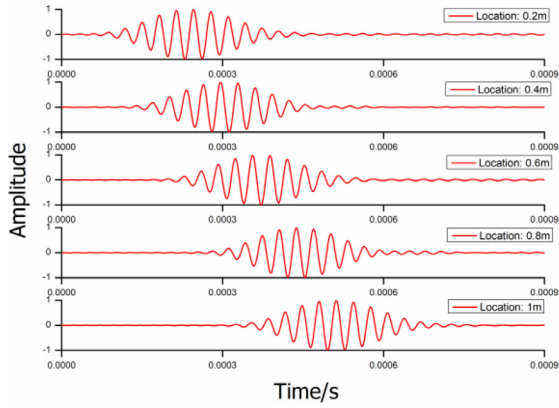


Fig. 29. Time-domain diagram of the signal at different measuring points.

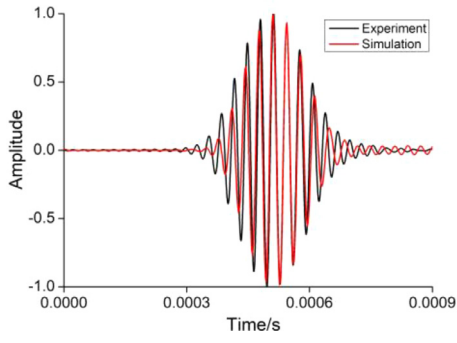


Fig. 30. Comparison diagram of received responses.

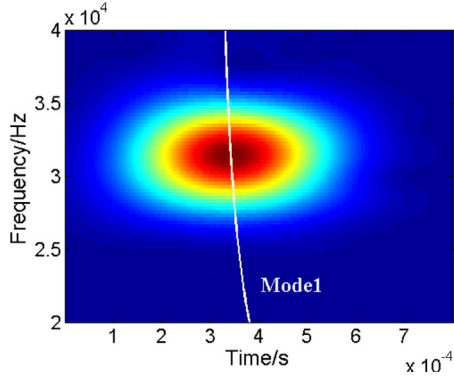


Fig. 31. Comparison of experimental results with time-frequency curve.

cross-sections. The curve was compared with the theoretical dispersion curve of the straight switch rail with a variable cross-section. The results show that the two are in good agreement with each other. This verifies the effectiveness of the analytical method.

- (3) Field testing and time-domain simulation were performed, revealing the propagation characteristics of Mode 1 in the straight switch rail. The results show that the two are in good agreement with each other, and that the group velocity is consistent with the group velocity obtained by the above method, verifying its effectiveness.
- (4) The article provides a method to study the guided wave propagation characteristics in straight switch rail with variable cross-section. Currently this method only gives a small amount of verification, while its applicability to other frequencies, wave modes and waveguides with different change rates has not been considered. Further research has yet to be conducted.

Declaration of Competing Interest

The authors declare that they have no known competing financial interests or personal relationships that could have appeared to influence the work reported in this paper.

CRediT authorship contribution statement

Rong Chen: Data curation, Methodology, Writing - original draft. **Chenyang Hu:** Conceptualization, Methodology, Software, Validation. **Jingmang Xu:** Supervision, Methodology. **Zheng Gong:** Visualization, Investigation. **Le Liu:** Software, Validation. **Ping Wang:** Writing - review & editing. **Xiaoping Chen:** Writing - review & editing.

Acknowledgments

The research and development effort has been supported by the Scientific Research Plan of China Railway (K2019G010), National Natural Science Foundation of China (51978586, 51778542, U1734207), Fundamental Research Funds for the Central Universities (2682018CX01) and Key Research and Development Projects of Science and Technology Program for Sichuan Province (2019YFG0283).

References

- [1] V. Giurgiutiu, Tuned Lamb wave excitation and detection with piezoelectric wafer active sensors for structural health monitoring, *J. Intell. Mater. Syst. Struct.* 16 (4) (2005) 291–305, doi:[10.1177/1045389X05050106](https://doi.org/10.1177/1045389X05050106).
- [2] V. Giurgiutiu, *Structural Health Monitoring with Piezoelectric Wafer Active Sensors*, Elsevier Academic Press, New York, 2008.
- [3] W.J. Staszewski, C. Boller, G. Tomlinson, *Health Monitoring of Aerospace Structures*, John Wiley & Sons, Chichester, 2004.
- [4] C.C. Ciang, J.R. Lee, H.J. Bang, Structural health monitoring for a wind turbine system: a review of damage detection methods, *Meas. Sci. Technol.* 19 (12) (2008) 310–314, doi:[10.1088/0957-0233/19/12/122001](https://doi.org/10.1088/0957-0233/19/12/122001).
- [5] N.M. Okasha, D.M. Frangopol, D. Saydam, L.W. Salvino, Reliability analysis and damage detection in high-speed naval craft based on structural health monitoring data, *Struct. Health Monit.* 9 (4) (2011) 361–379, doi:[10.1177/1475921710379516](https://doi.org/10.1177/1475921710379516).
- [6] K.F. Graff, *Wave Motion in Elastic Solids*, Clarendon PressUniversity Press, OxfordOxford, 1975.
- [7] J.D. Achenbach, *Wave Propagation in Elastic Solids*, Elsevier B.V., North Holland, 1975.
- [8] B.A. Auld, *Acoustic Fields and Waves in Solids*, J. Wiley, New York, 1973.
- [9] J.L. Rose, *Ultrasonic Guided Waves in Solid Media: Plates*, Cambridge University Press, Cambridge, 2014.
- [10] P. Zuo, X.D. Yu, Z. Fan, Acoustoelastic guided waves in waveguides with arbitrary prestress, *J. Sound Vib.* 469 (2020) 115113, doi:[10.1016/j.jsv.2019.115113](https://doi.org/10.1016/j.jsv.2019.115113).
- [11] Y. Wang, X. Li, Propagation characteristics and defect sensitivity analysis of guided wave from single excitation source in elbows, *IEEE Access* 7 (2019) 75542–75549, doi:[10.1109/ACCESS.2019.2920523](https://doi.org/10.1109/ACCESS.2019.2920523).
- [12] C.L. Lei, Q. Han, Y.J. Liu, X.C. Liu, B. Win, Investigation of wave propagation in double cylindrical rods considering the effect of prestress, *J. Sound Vib.* 353 (2015) 164–180, doi:[10.1016/j.jsv.2015.05.017](https://doi.org/10.1016/j.jsv.2015.05.017).
- [13] F. Krome, H. Gravenkamp, Analyzing modal behavior of guided waves using high order eigenvalue derivatives, *Ultrasonics* 71 (2016) 75–85, doi:[10.1016/j.ultras.2016.05.014](https://doi.org/10.1016/j.ultras.2016.05.014).
- [14] E. Kausel, P. Malishevsky, J. Barbosa, Osculations of spectral lines in a layered medium, *Wave Motion* 56 (2015) 22–42, doi:[10.1016/j.wavemoti.2015.01.004](https://doi.org/10.1016/j.wavemoti.2015.01.004).
- [15] X.N. Xu, Z. Lu, B. Xing, Z.J. Yu, An ultrasonic guided wave mode excitation method in rails, *IEEE Access* 6 (2018) 60414–60428, doi:[10.1109/ACCESS.2018.2875123](https://doi.org/10.1109/ACCESS.2018.2875123).
- [16] M.J.S. Lowe, Matrix techniques for modeling ultrasonic waves in multilayered media, *IEEE Trans. Ultrasonics Ferroelectrics Freq. Control* 42 (4) (1995) 525–542, doi:[10.1109/58.393096](https://doi.org/10.1109/58.393096).
- [17] E. Kausel, Dynamic point sources in laminated media via the thin-layer method, *Int. J. Solids Struct.* 36 (31) (1999) 4725–4742, doi:[10.1016/S0020-7683\(98\)00262-5](https://doi.org/10.1016/S0020-7683(98)00262-5).
- [18] E. Kausel, Thin-layer method: formulation in the time domain, *Int. J. Numer. Methods Eng.* 37 (1994) 927–941, doi:[10.1002/nme.1620370604](https://doi.org/10.1002/nme.1620370604).
- [19] E. Kausel, *Forced Vibrations of Circular Foundations on Layered Media*, Research report (1974).
- [20] L. Gavrić, Computation of propagative waves in free rail using a finite element technique, *J. Sound Vib.* 185 (3) (1995) 531–543, doi:[10.1006/jsvi.1995.0398](https://doi.org/10.1006/jsvi.1995.0398).
- [21] M. Castaings, M. Lowe, Finite element model for waves guided along solid systems of arbitrary section coupled to infinite solid media, *J. Acoust. Soc. Am.* 123 (2) (2008) 696–708, doi:[10.1121/1.2821973](https://doi.org/10.1121/1.2821973).
- [22] Š. Sorohan, N. Constantin, M. Găvan, V. Anghel, Extraction of dispersion curves for waves propagating in free complex waveguides by standard finite element codes, *Ultrasonics* 51 (4) (2011) 503–515, doi:[10.1016/j.ultras.2010.12.003](https://doi.org/10.1016/j.ultras.2010.12.003).
- [23] T. Hayashi, W.J. Song, J.L. Rose, Guided wave dispersion curves for a bar with an arbitrary cross-section, a rod and rail example, *Ultrasonics* 41 (3) (2003) 175–183, doi:[10.1016/S0041-624X\(03\)00097-0](https://doi.org/10.1016/S0041-624X(03)00097-0).
- [24] I. Bartoli, A. Marzani, F.L.D. Scalea, E. Viola, Modeling wave propagation in damped waveguides of arbitrary cross-section, *J. Sound Vib.* 295 (3–5) (2006) 685–707, doi:[10.1016/j.jsv.2006.01.021](https://doi.org/10.1016/j.jsv.2006.01.021).
- [25] M. Cong, X.J. Wu, J.X. Wu, R. Liu, Dispersion analysis of guided waves in the finned tube using the semi-analytical finite element method, *J. Sound Vib.* 401 (2017) 114–126, doi:[10.1016/j.jsv.2017.04.037](https://doi.org/10.1016/j.jsv.2017.04.037).
- [26] H. Gravenkamp, C. Song, J. Prager, A numerical approach for the computation of dispersion relations for plate structures using the scaled boundary finite element method, *J. Sound Vib.* 331 (11) (2012) 2543–2557, doi:[10.1016/j.jsv.2012.01.029](https://doi.org/10.1016/j.jsv.2012.01.029).
- [27] Y. Liu, Q. Han, C. Li, X. Liu, B. Wu, Guided wave propagation and mode differentiation in the layered magneto-electro-elastic hollow cylinder, *Compos. Struct.* 132 (2015) 558–566, doi:[10.1016/j.compstruct.2015.05.074](https://doi.org/10.1016/j.compstruct.2015.05.074).
- [28] L. Elmaimouni, J.E. Lefebvre, V. Zhang, T. Gryba, A polynomial approach to the analysis of guided waves in anisotropic cylinders of infinite length, *Wave Motion* 42 (2) (2005) 177–189, doi:[10.1016/j.wavemoti.2005.01.005](https://doi.org/10.1016/j.wavemoti.2005.01.005).
- [29] H. Cunfu, L. Hongye, L. Zhenghua, W. Bin, The propagation of coupled Lamb waves in multilayered arbitrary anisotropic composite laminates, *J. Sound Vib.* 332 (26) (2013) 7243–7256, doi:[10.1016/j.jsv.2013.08.035](https://doi.org/10.1016/j.jsv.2013.08.035).
- [30] Y. Jiangong, W. Bin, H. Cunfu, Circumferential thermoelastic waves in orthotropic cylindrical curved plates without energy dissipation, *Ultrasonics* 50 (3) (2010) 416–423, doi:[10.1016/j.ultras.2009.09.031](https://doi.org/10.1016/j.ultras.2009.09.031).
- [31] J.L. Rose, M.J. Avioli, P. Mudge, R. Sanderson, Guided wave inspection potential of defects in rail, *NDT & E Int.* 37 (2) (2004) 153–161, doi:[10.1016/j.ndteint.2003.04.001](https://doi.org/10.1016/j.ndteint.2003.04.001).

- [32] P.W. Loveday, Semi-analytical finite element analysis of elastic waveguides subjected to axial loads, *Ultrasonics* 49 (3) (2009) 298–300, doi:[10.1016/j.ultras.2008.10.018](https://doi.org/10.1016/j.ultras.2008.10.018).
- [33] X. Duan, L. Zhu, Z. Yu, X.N. Xu, Estimating the axial load of in-service continuously welded rail under the influences of rail wear and temperature, *IEEE Access* 7 (2019) 143524–143538, doi:[10.1109/ACCESS.2019.2945609](https://doi.org/10.1109/ACCESS.2019.2945609).
- [34] P.W. Loveday, Guided wave inspection and monitoring of railway track, *J. Nondestr. Eval.* 31 (4) (2012) 303–309, doi:[10.1007/s10921-012-0145-9](https://doi.org/10.1007/s10921-012-0145-9).
- [35] F. Burger, P. Loveday, Ultrasonic broken rail detector and rail condition monitor technology, in: *Proceedings of the 11th International Heavy Haul Association Conference (IHHA 2017), Cape Town, South Africa, 2017*, pp. 275–280.
- [36] P.W. Loveday, C.S. Long, D.A. Ramatlo, Ultrasonic guided wave monitoring of an operational rail track, *Struct. Health Monit.* 19 (6) (2019) 1666–1684, doi:[10.1177/1475921719893887](https://doi.org/10.1177/1475921719893887).
- [37] D.A. Ramatlo, C.S. Long, P.W. Loveday, D.N. Wilke, A modelling framework for simulation of ultrasonic guided wave-based inspection of welded rail tracks, *Ultrasonics* 108 (2020), doi:[10.1016/j.ultras.2020.106215](https://doi.org/10.1016/j.ultras.2020.106215).
- [38] P. Cawley, M.J.S. Lowe, D.N. Alleyne, B. Pavlakovic, P. Wilcox, Practical long range guided wave testing: applications to pipes and rail, *Mater. Eval.* 61 (1) (2003) 66–74.
- [39] J.L. Rose, M.J. Avioli, Y. Cho, Elastic wave analysis for broken rail detection, *Rev. Quant. Nondestr. Eval.* 21 (2002) 1806–1812.
- [40] S. Moustakidis, V. Kappatos, P. Karlsson, C. Selcuk, T.H. Gan, K. Hrissagis, An intelligent methodology for railways monitoring using ultrasonic guided waves, *J. Nondestr. Eval.* 33 (4) (2014) 694–710, doi:[10.1007/s10921-014-0264-6](https://doi.org/10.1007/s10921-014-0264-6).
- [41] S. Huang, S. Wang, W. Li, Q. Wang, *Electromagnetic Ultrasonic Guided Waves*, Springer, Singapore, 2016, doi:[10.1007/978-981-10-0564-0](https://doi.org/10.1007/978-981-10-0564-0).
- [42] I.I. Setschedi, P.W. Loveday, C.S. Long, D.N. Wilke, Estimation of rail properties using semi-analytical finite element models and guided wave ultrasound measurements, *Ultrasonics* 96 (2019) 240–252, doi:[10.1016/j.ultras.2018.12.015](https://doi.org/10.1016/j.ultras.2018.12.015).
- [43] M. Sun, Y. Wang, X. Zhang, Y. Liu, N. Feng, Feature selection and classification algorithm for non-destructive detecting of high-speed rail defects based on vibration signals, *Instrumentation & Measurement Technology Conference, IEEE*, 2014.
- [44] Y. Gharaibeh, R. Sanderson, P. Mudge, C. Ennaceur, W. Balachandran, Investigation of the behaviour of selected ultrasonic guided wave modes to inspect rails for long-range testing and monitoring, *Proc. Inst. Mech. Eng. Part F J. Rail Rapid Transit* 1 (F3) (2011) 1–14, doi:[10.1243/09544097JRRT413](https://doi.org/10.1243/09544097JRRT413).
- [45] P.W. Loveday, C.S. Long, Laser vibrometer measurement of guided wave modes in rail track, *Ultrasonics* 57 (2015) 209–217, doi:[10.1016/j.ultras.2014.11.010](https://doi.org/10.1016/j.ultras.2014.11.010).
- [46] V. Pagneux, A. Maurel, Lamb wave propagation in elastic waveguides with variable thickness, *Proc. R. Soc. A* 462 (2068) (2006) 1315–1339, doi:[10.1098/rspa.2005.1612](https://doi.org/10.1098/rspa.2005.1612).
- [47] A. Maurel, J.F. Mercier, S. Félix, Propagation in waveguides with varying cross section and curvature: a new light on the role of supplementary modes in multi-modal methods, *Proc. R. Soc. A* 470 (2166) (2014) 20140008, doi:[10.1098/rspa.2014.0008](https://doi.org/10.1098/rspa.2014.0008).
- [48] M.E.C. El-Kettani, F. Lupppé, A. Guillet, Guided waves in a plate with linearly varying thickness: experimental and numerical results, *Ultrasonics* 42 (1–9) (2004) 807–812, doi:[10.1016/j.ultras.2004.01.071](https://doi.org/10.1016/j.ultras.2004.01.071).
- [49] P. Marical, M.E.C. El-Kettani, M.V. Predoi, Guided waves in elastic plates with Gaussian section variation: experimental and numerical results, *Ultrasonics* 47 (1–4) (2007) 1–9, doi:[10.1016/j.ultras.2007.05.004](https://doi.org/10.1016/j.ultras.2007.05.004).
- [50] Q. Deng, Z. Yang, Propagation of guided waves in bonded composite structures with tapered adhesive layer, *Appl. Math. Model.* 35 (11) (2001) 5369–5381, doi:[10.1016/j.apm.2011.04.042](https://doi.org/10.1016/j.apm.2011.04.042).
- [51] L. De Marchi, A. Marzani, N. Speciale, E. Viola, Prediction of pulse dispersion in tapered waveguides, *NDT & E Int.* 43 (3) (2010) 265–271, doi:[10.1016/j.ndteint.2009.12.004](https://doi.org/10.1016/j.ndteint.2009.12.004).
- [52] L. De Marchi, A. Marzani, M. Miniaci, A dispersion compensation procedure to extend pulse-echo defects location to irregular waveguides, *NDT & E Int.* 54 (2013) 115–122, doi:[10.1016/j.ndteint.2012.12.009](https://doi.org/10.1016/j.ndteint.2012.12.009).
- [53] L. Moreau, J.G. Minonzio, M. Talmant, M. Laugier, Measuring the wavenumber of guided modes in waveguides with linearly varying thickness, *J. Acoust. Soc. Am.* 135 (5) (2014) 2614–2624, doi:[10.1121/1.4869691](https://doi.org/10.1121/1.4869691).
- [54] C. Höhne, J. Prager, Simulation of ultrasound propagation in waveguides with non-constant thickness by a multimodal approach, *Forum Acusticum* (2014) 1–6.
- [55] C. Höhne, Multimodal Approach for the Numerical Simulation of Ultrasonic Guided Waves in Cylindrical Structures of Non-Constant Thickness, PhD thesis, Technischen Universität Cottbus-Senftenberg (2016).
- [56] F. Krome, H. Gravenkamp, C. Birk, Prismatic semi-analytical elements for the simulation of linear elastic problems in structures with piecewise uniform cross section, *Comput. Struct.* 192 (2017) 83–95, doi:[10.1016/j.compstruc.2017.06.015](https://doi.org/10.1016/j.compstruc.2017.06.015).
- [57] H. Gravenkamp, Efficient simulation of elastic guided waves interacting with notches, adhesive joints, delaminations and inclined edges in plate structures, *Ultrasonics* 82 (2017) 101–113, doi:[10.1016/j.ultras.2017.07.019](https://doi.org/10.1016/j.ultras.2017.07.019).
- [58] J. Zhang, H. Ma, W. Yan, Z.J. Li, Defect detection and location in switch rails by acoustic emission and Lamb wave analysis: a feasibility study, *Appl. Acoustics* 105 (2016) 67–74, doi:[10.1016/j.apacoust.2015.11.018](https://doi.org/10.1016/j.apacoust.2015.11.018).
- [59] J. Wu, Z. Tang, F. Lv, K.J. Yang, Ultrasonic guided wave-based switch rail monitoring using independent component analysis, *Meas. Sci. Technol.* 29 (11) (2018) 115102, doi:[10.1088/1361-6501/adc47](https://doi.org/10.1088/1361-6501/adc47).
- [60] P. Wang, X.C. Ma, J.M. Xu, J. Wang, R. Chen, Numerical investigation on effect of the relative motion of stock/switch rails on the load transfer distribution along the switch panel in high-speed railway turnout, *Veh. Syst. Dyn.* 57 (2) (2019) 226–246, doi:[10.1080/00423114.2018.1458992](https://doi.org/10.1080/00423114.2018.1458992).
- [61] F. Moser, L.J. Jacobs, J. Qu, Modeling elastic wave propagation in waveguides with the finite element method, *NDT&E Int.* 2 (4) (1999) 225–234, doi:[10.1016/S0963-8695\(98\)00045-0](https://doi.org/10.1016/S0963-8695(98)00045-0).
- [62] D. Alleyne, A two-dimensional Fourier transform method for the measurement of propagating multimode signals, *J. Acoust. Soc. Am.* 89 (3) (1991) 1159, doi:[10.1121/1.400530](https://doi.org/10.1121/1.400530).
- [63] J.J. Ditri, J.L. Rose, Excitation of guided elastic wave modes in hollow cylinders by applied surface tractions, *J. Appl. Phys.* 72 (7) (1992) 2589–2597, doi:[10.1063/1.351558](https://doi.org/10.1063/1.351558).